RSC Advances

PAPER

View Article Online
View Journal | View Issue

Cite this: *RSC Adv.*, 2025, **15**, 32810

Morphology and interfacial design of SnO_2 thin-film anodes for high-performance lithium-ion batteries

Mukagali Yegamkulov,[ab] Zhansaya Bakhytzhanova,[ac] Ayazhan Bekmakhanova,[ac] Nurbolat Issatayev,[abd] Arailym Nurpeissova,[ab] Zhumabay Bakenov[abd] and Aliya Mukanova[*ab]

The continuous demand for high-performance lithium-ion batteries (LIBs) has accelerated the development of microscale energy storage systems with improved specific and volumetric capacities. Tin oxide (SnO_2) is a promising anode material due to its high theoretical capacity and favorable lithiation properties; however, its practical application is hindered by significant volume changes and unstable electrode–electrolyte interfaces during cycling. Here, we systematically investigate the impact of thin film morphology and artificial interface engineering on the electrochemical performance of radio frequency (RF) magnetron-sputtered SnO_2 anodes. By optimizing deposition and annealing parameters, we achieve porous SnO_2 architectures with enhanced cycling stability. A subsequent carbon coating reduces electrolyte contact and buffers volume expansion, while the incorporation of 5 wt% vinylene carbonate (VC) into the electrolyte enables the formation of a robust, elastic solid electrolyte interphase (SEI). The dual approach – combining engineered porosity with interfacial stabilization – significantly improved capacity retention, suppressed polarization, and ensured high coulombic efficiency over 200 cycles. Post-mortem scanning electron microscope (SEM) and X-ray photoelectron spectroscopy (XPS) analyses confirm that the carbon coating and VC worked synergistically to preserve structural integrity, minimized side reactions, and promoted favorable SEI composition. These results highlight an effective strategy for designing durable, high-capacity SnO_2-based thin film anodes for next-generation LIBs.

Received 27th July 2025
Accepted 1st September 2025

DOI: 10.1039/d5ra05444c

rsc.li/rsc-advances

1 Introduction

Lithium-ion batteries (LIBs) are widely recognized as satisfactory solutions for powering numerous devices, owing to their low self-discharge rate, long cycle life and high conversion efficiency, and the ease with which they can be fabricated into flexible designs.[1–3] Increasing demands for specific power and energy density are driving the development of LIBs with improved performance.[4] In this context, particular attention is being paid to microscale energy storage systems, where compactness, high energy efficiency, and stable operation in a limited volume are critical. To meet these evolving requirements, it is crucial to develop active thin film materials that offer improved specific and volumetric capacities.[1,5] Currently, the main research focus is on two key classes of anode materials: metal oxides and carbons.[6–9]

Among various metal oxides, tin oxide (SnO_2) stands out as a very promising anode material for LIBs due to its high theoretical capacity of 1494 mAh g^{-1}, which significantly exceeds the value of metallic Sn, as well as its resistance to oxidation and environmental safety.[10,11] Electrochemical lithiation of SnO_2 anodes typically occurs through three sequential processes, each associated with different voltage ranges and capacitance contributions, as described below:

$$\text{Insertion: } SnO_2 + xLi^+ + xe^- \rightleftarrows Li_xSnO_2 \quad (1)$$

$$\text{Conversion: } SnO_2 + 4Li^+ + 4e^- \rightleftarrows Sn + 2Li_2O \quad >1.2\ \text{V } \textit{vs.}\ Li/Li^+ \text{ with } \approx 711\ \text{mAh g}^{-1} \quad (2)$$

$$\text{Alloying/dealloying: } Sn + xLi^+ + xe^- \rightleftarrows Li_xSn\ (0 \le x \le 4.4) \quad >0.5\ \text{V } \textit{vs.}\ Li/Li^+ \text{ with } \approx 783\ \text{mAh g}^{-1} \quad (3)$$

A transformation reaction occurs at relatively moderate potentials (~1.2 V and 0.5 V *vs.* Li/Li^+).[12] These potentials help to reduce the likelihood of lithium plating on the anode and minimize polarization. The high electrical conductivity of the

[a]*National Laboratory Astana, Nazarbayev University, Kabanbay Batyr Ave. 53, Astana 010000, Kazakhstan. E-mail: aliya.mukanova@nu.edu.kz*
[b]*Institute of Batteries LLC, Kabanbay Batyr Ave. 53, Astana 010000, Kazakhstan*
[c]*Department of Chemistry, Faculty of Nature Sciences, L.N. Gumilyov Eurasian National University, Satbayev str. 2, Astana 010000, Kazakhstan*
[d]*Department of Chemical and Materials Engineering, School of Engineering and Digital Sciences, Nazarbayev University, Kabanbay Batyr Ave. 53, Astana 010000, Kazakhstan*

lithiated phases and the ability of SnO_2 to form stable nanostructures determine its overall effectiveness.

The practical use of SnO_2-based anodes is limited by a large volumetric expansion (~250%) during lithiation and delithiation, which induces mechanical stress, damages the electrode structure, and reduces cyclic stability.[13] Additionally, such drastic volume changes disrupt the formed solid electrolyte interphase (SEI), forcing its continual reformation. This leads to ongoing Li and electrolyte consumption and further degrades electrochemical performance.[14] Maintaining a durable, stable SEI layer is thus essential both for preserving electrode integrity and preventing continued electrolyte decomposition.

Fine-tuning radio frequency (RF) magnetron sputtering parameters – such as sputtering power, working pressure, substrate temperature, and Ar/O_2 ratio – can allow to tailor SnO_2 thin film morphology that effectively buffers volumetric changes during lithiation/delithiation. Prior studies of porous SnO_2 nanostructures have shown that uniform pores (2–30 nm) yield high reversible capacities (up to ~645 mAh g^{-1}) and excellent retention (~95%) over 100 cycles.[15] In magnetron-deposited metal oxides, increased sputtering power and pressure can enhance adatom mobility, promote grain boundary formation, and introduce voided or columnar morphologies. By optimizing these variables, we anticipate achieving a porous SnO_2 architecture that can maintain structural integrity and deliver improved lithium storage performance in thin film anodes.[16] Moreover, magnetron sputtering, as used in this study (Table TS1), is considered a scalable technique since its parameters (gas flow, RF power, pressure, and substrate temperature) can be precisely controlled and adapted to large-area substrates. This makes it widely applicable in industrial coating processes, although the relatively high cost and lower deposition rates compared with solution-based methods may limit its scalability.

Carbon (C) coatings on SnO_2 significantly reduce the direct exposure of the active material to the electrolyte, making them more inert than bare SnO_2. This helps suppress unwanted electrolyte decomposition during cycling and promotes a more stable SEI formation.[17] Vinylene carbonate (VC) preferentially decomposes in the first few cycles, forming a dense, elastic, and chemically robust SEI.[18,19] This SEI prevents continuous electrolyte breakdown, curtails formation of resistive byproducts, and maintains high coulombic efficiency (CE). Together, carbon coating and VC additive are capable to reinforce SEI integrity – mechanically, electronically, and chemically – leading to substantially improved cycling performance of SnO_2-based anodes. In contrast to prior studies that used either carbon coatings or VC alone, our work establishes a coupled design rule: a crack-tolerant porous microstructure (*via* sputter/anneal control) combined with an amorphous carbon shell plus VC to yield a LiF-rich, elastic SEI. To our knowledge, such an integrated morphology-plus-SEI strategy has not been previously reported.

In contrast to prior SnO_2 studies that applied either carbon coatings or VC additives in isolation, our work establishes a coupled design rule for thin-film SnO_2 anodes: (i) first engineer a crack-tolerant, porous microstructure *via* sputter/anneal control to minimize polarization and accommodate strain, and (ii) then stabilize the interface by combining an amorphous ~20 nm carbon shell with 5 wt% VC to build a LiF-rich, elastic SEI. To our knowledge, such an integrated morphology-plus-SEI strategy, demonstrated on RF-sputtered thin films with controlled loading, and supported by a full electrochemistry-EIS-XPS/SEM evidence chain, has not been reported.

In this study, we systematically investigated SnO_2 thin film anodes fabricated *via* RF magnetron sputtering, focusing on how deposition conditions can be optimized to engineer a porous architecture that buffers volume expansion during lithiation/delithiation. By tuning sputtering parameters, we aim to foster a porosity and grain boundaries, enhancing structural resilience and ion storage. Following this, we applied a carbon coating to reduce direct SnO_2 – electrolyte contact – thus suppressing parasitic reactions – and introduced 5 wt% VC in the electrolyte to form a dense, elastic SEI. Our results reveal that this dual strategy – morphology *via* sputtering and interfacial stabilization *via* C-coating + VC – significantly improves cyclic stability, electronic conductivity, demonstrating a promising route for high-performance SnO_2-based thin film anodes.

2 Experimental part

2.1. Material preparation

SnO_2 anode thin films were deposited by radio frequency (RF) magnetron sputtering (Angstrom Engineering Inc.) using the Sn metallic target (5.08 cm diameter × 0.635 cm thick, 99.994–99.999% pure, Kurt J. Lesker Company) in the mixture of high purity Ar and O_2 (15 : 15 sccm) gases. The substrate used was a pre-cleaned stainless steel (SS) spacer with a diameter of 15.8 mm and a thickness of 0.5 mm from AME Energy, onto which an intermediate layer of titanium (~10 nm Ti) was deposited from Ti target (Kurt J. Lesker Company) to enhance the adhesion of the active layer to the substrate. The process was carried out at a base pressure below 2×10^{-6} torr, deposition pressure of 5 mTorr, at a power of 60 W (~2.96 W cm^{-2}), at room temperature (RT) and at 300 °C (Table TS1) and a substrate rotation speed of 10 rpm, which contributed to the formation of a uniform deposition with an active mass in the range of 0.55–0.65 mg. To eliminate surface contaminations and to provide a consistent target voltage, the Sn target was pre-sputtered in the Ar and O_2 atmospheres for 20 minutes before deposition.

Then, the SnO_2 films deposited on SS at RT and at 300 °C followed by annealing at 620 °C for 2 hours at a heating rate of 10 °C min^{-1} in ambient atmosphere in muffle furnace to foster structure and morphology. After annealing, the samples were cooled naturally to RT. For convenience, the SnO_2 samples deposited at RT and 300 °C were denoted as SnO_2-RT and SnO_2-300, respectively. The post-annealed films were labeled as SnO_2-RT-620 and SnO_2-300-620 as presented in Table TS2. The deposition rate of the films was monitored by INFICON Quartz Crystal Monitor (QCM) and the mass of thin films were checked with ultra-microbalance before and after sputtering/annealing of thin films (Mettler Toledo XP2U Ultra Microbalance). The mass of the samples was in the range of 0.55–0.65 mg.

A Turbo Coater AGB7232 (Agar Scientific, UK) was used as the carbon coating system for single-time coating of as-deposited and annealed SnO_2 thin films without any annealing after C-coating. The samples of the modified SnO_2 (by C coating and VC adding) thin film electrodes were marked as SnO_2–C and SnO_2–C–VC (Table TS3).

2.2. Material characterization

To study the structure and morphology of the samples, their comprehensive physicochemical characterization was done using various analytical methods. Morphological analysis was carried out using scanning electron microscopy (SEM, JEOL JSM-IT800, Japan) and a transmission electron microscope (TEM, JEOL JEM-1400 Plus, JEOL, Peabody, MA, USA). The crystal structure was studied by X-ray diffraction (XRD) on a SmartLab (Rigaku) setup using Cu Kα radiation ($\lambda_{CuK\alpha1}$ = 1.54056 Å, $\lambda_{CuK\alpha2}$ = 1.54439 Å) in the Bragg–Brentano reflection geometry. The XRD data were obtained over a 2θ range from 5 to 70° at a scan rate of 5° min^{-1} using 40 kV, 30 mA X-ray. X-ray photoelectron spectroscopy (XPS) (Shimazu-Kratos Analytical, UK) was utilized to investigate the elemental composition and oxidation states of the samples.

For post-mortem characterization by SEM and XRD, cycled electrodes were washed with ethyl methyl carbonate (EMC), whereas unwashed electrodes were used for elemental composition analysis (XPS).

2.3. Electrochemical investigations

The CR2032 galvanic cells have been assembled with the obtained thin-film SnO_2 anodes. A Celgard 2400 polypropylene membrane was used as a separator and lithium metal chips (99.9% MTI Co.) as an opposite and reference electrode. The assembly was carried out in an Ar-sealed glove box (MBRAUN LABMaster Pro, Germany) under a high-purity argon atmosphere with <0.1 ppm H_2O and <0.1 ppm O_2 to avoid moisture and oxygen contamination. A commercial 1 M $LiPF_6$ in a mixture of ethyl carbonate (EC), dimethyl carbonate (DEC), and ethyl methyl carbonate (EMC) (1 : 1 : 1 by vol%) was used as the bare electrolyte. To obtain an electrolyte with the addition of VC, 5 wt% VC was added to the commercial electrolyte, followed by mixing in a glove box filled with argon.

Electrochemical testing was performed using cyclic voltammetry and potentiostatic electrochemical impedance spectroscopy (CV, PEIS, VMP3, BioLogic Instruments, France) and galvanostatic charge–discharge cycling with a multichannel battery testing system (Neware Co., Shenzhen, China) at a 0.1C rate (1C = 1494 mAh g^{-1}) within a potential range of 0.01 to 3 V *vs.* Li^+/Li.

3 Results and discussions

All SnO_2 thin film electrodes were prepared by RF magnetron sputtering from a metallic Sn target onto Ti-coated SS substrates using an Ar/O_2 gas mixture (15 : 15 sccm) under a constant pressure of 5 mTorr. Amorphous SnO_2 is generally reported to offer superior cycling performance due to its structural flexibility and enhanced ability to accommodate volume changes during lithiation and delithiation.[20] In this study, both amorphous and crystalline forms of tin oxide were systematically investigated. Sputtering was performed at either RT and 300 °C to examine how deposition temperature influences the film's morphology, crystallinity, and, most importantly, electrochemical behavior. To further promote crystallization and morphology, the as-deposited films underwent annealing at 620 °C. After figuring out the optimal condition, the superior-performance electrode was used further as a base for artificial SEI engineering.

3.1. The effect of deposition and post-annealing conditions on SnO_2 thin film anode cycling performance

In order to clarify the influence of deposition parameters and subsequent heat treatment on the properties of SnO_2 thin films, a comprehensive analysis of their structure, surface morphology, and electrochemical behavior was carried out. Fig. 1 shows the XRD patterns of the films obtained under different conditions: immediately after deposition, as well as after subsequent annealing. From the XRD patterns, it can be seen that the SnO_2 films obtained at RT and 300 °C exhibit different crystal structure. While the former demonstrates slight broad peak ascribed to amorphous or nanocrystalline structure, the latter became crystallized during deposition, as evidenced by the appearance of clearly defined reflections corresponding to the tetragonal structure of SnO_2 (JCPDS card no. 00-041-1445), including diffraction peaks at 2θ = ~26.7° (110), ~33.9° (101), ~37.9° (200), ~51.7° (211) and ~66.2° (301).[21] This is due to the fact that the relatively high substrate temperature during deposition promotes the diffusion of atoms and their ordered arrangement in the crystal lattice, which leads to the formation of the tetragonal phase of SnO_2 already during the film growth. An annealing at 620 °C led to obvious crystallization of the amorphous SnO_2-RT,[20,22] but did not affect much already crystallized SnO_2-300. The absence of any extraneous peaks in the films indicates their phase purity after heat treatment in air.

The surface morphology was analyzed by scanning electron microscopy. SEM images (Fig. 1c–e) show the morphology of SnO_2 films under different deposition and annealing conditions. The SnO_2-RT sample, as shown in the top view (Fig. 1b), has a dense structure with uniformly distributed nanoclusters. This observation is further supported by the cross-sectional SEM image (Fig. FS1a), which shows a well-defined columnar structure with vertically aligned grains and narrow inter-columnar spaces, characteristic of films deposited at low substrate temperatures. After annealing in air (Fig. 1c), the structure became more uniform and granular, indicating improved porosity and the formation of microcracks.[23] Meanwhile, the sample deposited at 300 °C (Fig. 1d) has a more distinct granular structure due to thermal activation of grain growth during deposition. The subsequent annealing (Fig. 1e) enhanced the surface granulation and crystallinity. Thus, both the deposition temperature and the post-annealing significantly affected the morphology and structure of the films.

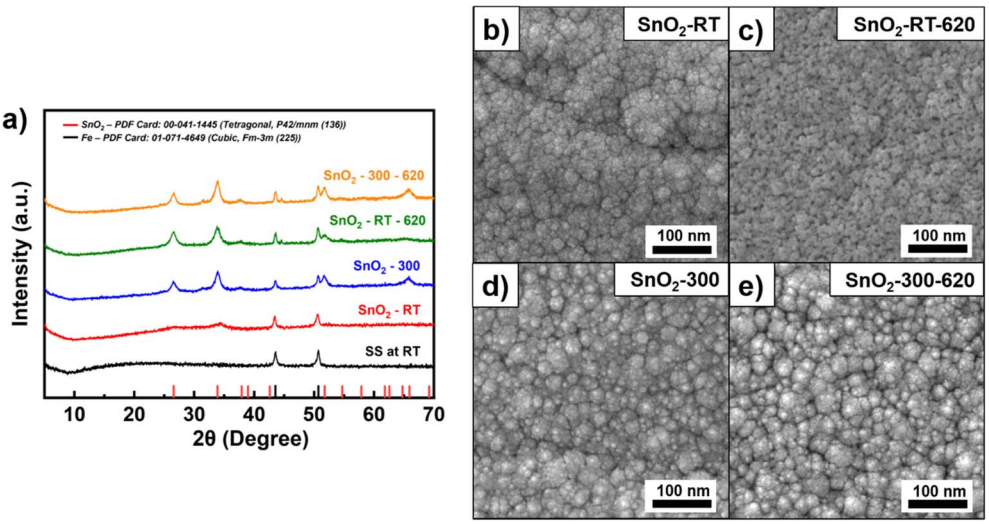

Fig. 1 (a) XRD patterns of SnO_2 thin films deposited under different conditions; SEM surface images of SnO_2 thin films (b) SnO_2-RT, (c) SnO_2-RT-620, (d) SnO_2-300, (e) SnO_2-300-620.

The reduction in particle size might positively contribute to the mechanical stability of the anode due to the uniform distribution of mechanical stresses arose from volume changes during lithiation and delithiation. The fine-grained structure usually reduces the tendency to aggregation, ensures reversible volume changes, and maintains the integrity of the material during cycling. In this context, samples annealed in air at high temperatures and possessing a homogeneous porous morphology are expected to demonstrate the greatest potential in terms of capacity and cyclic stability.

The lithiation behavior of the SnO_2 thin film electrodes was thoroughly examined through galvanostatic charge–discharge profiles (Fig. 2a and b), CV (Fig. 2c), and differential capacity (dQ/dV, Fig. 2d), all of which consistently reflect the characteristic three-step reaction mechanism of SnO_2-based anodes. During the first discharge cycle, at potentials above 1.2–1.5 V, Li^+ ions are inserted into the SnO_2 crystal lattice with the formation of intermediate compounds of the Li_xSnO_2 type (eqn (1)), which is accompanied by a smooth decrease in potential. A distinct plateau at approximately 1.2 V is observed in all samples, corresponding to the irreversible conversion of SnO_2 to metallic Sn and Li_2O (eqn (2)). This process is accompanied by SEI formation and accounts for the initial irreversible capacity loss.[24] Upon further discharge below 0.5 V, a broad plateau or peak arises from the alloying of lithium with Sn to form Li_xSn ($0 \leq x \leq 4.4$) (eqn (3)), which is the primary contributor to capacity in subsequent cycles (Fig. 2a and b). The CV curves in Fig. 2c exhibit a cathodic peak around 0.8 V (conversion) and a broad feature below 0.5 V (alloying), while dQ/dV analysis in Fig. 2d reveals corresponding cathodic and anodic peaks near 0.8 V and 0.6/1.3 V, respectively. In the charging process, a gradual potential increase in the range of 0.2–1.5 V reflects the dealloying of Li_xSn and partial reoxidation of Sn.[25] The anodic peaks at ~0.6 V (dealloying) persist across multiple cycles, indicating reversible behavior, whereas the diminishing intensity of the ~1.3 V peak suggests that the reformation of SnO_2 is largely irreversible. Collectively, these electrochemical features confirm that after the initial cycle, the capacity is predominantly governed by the highly reversible alloying/dealloying reaction between Li and Sn.

Among the studied electrodes, the SnO_2 film deposited at room temperature and post-annealed in air (SnO_2-RT-620, blue curve) exhibited the most outstanding performance. In the first cycle (Fig. 2a), it delivered the highest discharge capacity of approximately 1623 mAh g^{-1}, with well-defined plateaus corresponding to the conversion of SnO_2 to Sn and subsequent alloying with Li^+, indicating efficient reaction kinetics and high active material utilization. The superior performance of the SnO_2-RT-620 electrode can be attributed to its crystal and morphological structure.

As confirmed by XRD (Fig. 1a), annealing induced the crystallization of initially amorphous SnO_2 into a well-defined tetragonal phase. Additionally, SEM image (Fig. 1c) reveals a more homogeneous and porous morphology, which promotes Li^+ diffusion, buffers volume changes during cycling, and ensures the mechanical stability of the electrode – factors collectively contributing to improved cycling stability. Impressively, even after 50 cycles (Fig. 1c), the SnO_2-RT-620 electrode retained a capacity of about 795 mAh g^{-1}, nearly twice that of the next-best sample, and maintained a stable potential profile, reflecting the formation of a robust SEI and good structural integrity.

By contrast, the SnO_2 sample deposited at 300 °C and annealed in air (SnO_2-300-620, green curve) showed a lower initial capacity (~1398 mAh g^{-1}), yet better retention than the non-air-annealed counterparts, maintaining ~252 mAh g^{-1} after 50 cycles. The moderate performance of this electrode suggests that while elevated deposition temperature aids crystallinity, the air-annealing step is still crucial for optimizing electrochemical activity and stability.

The samples deposited without air annealing showed inferior behavior. The SnO_2-300 anode (red curve) exhibited an

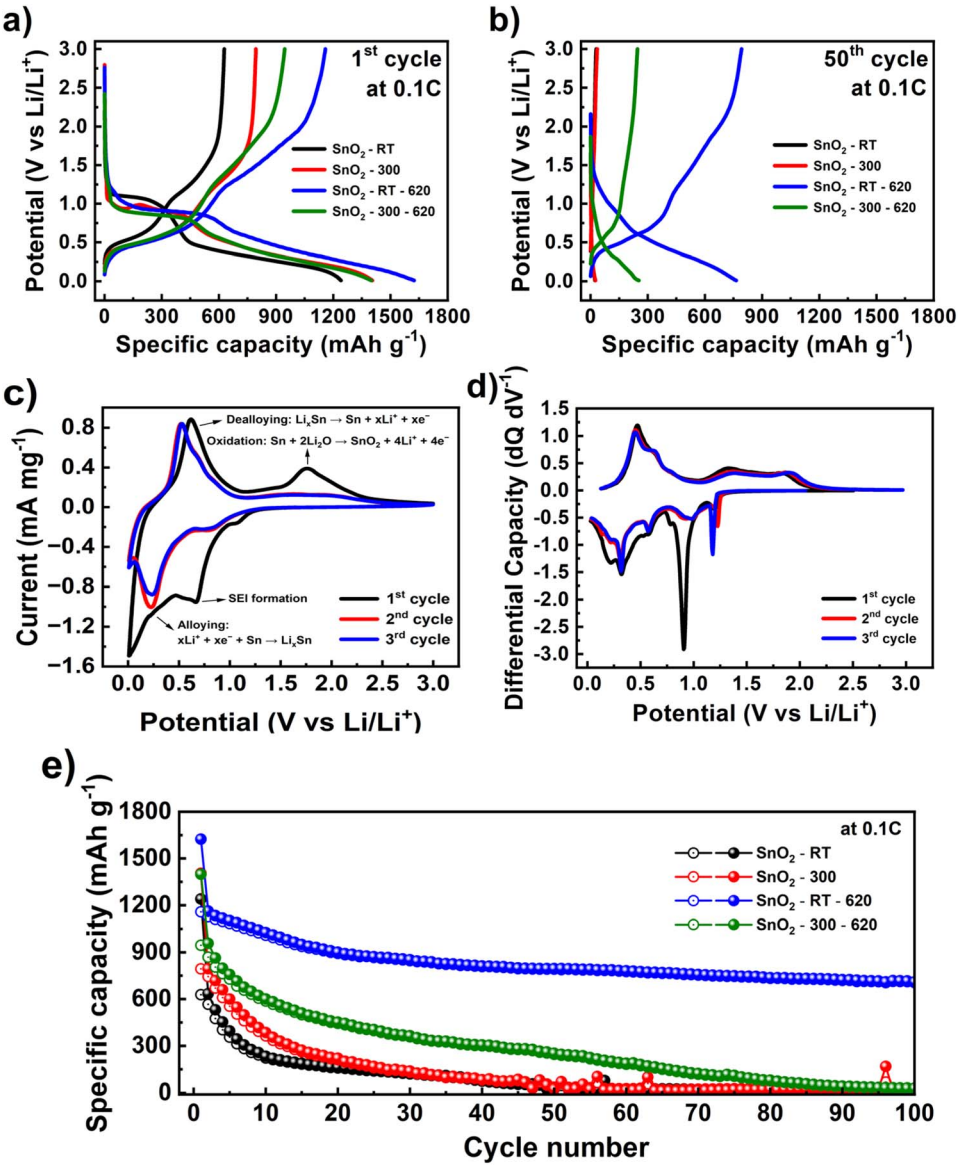

Fig. 2 Potential profiles of all samples at 0.1C in (a) 1st and (b) 50th cycles, (c) CV of SnO_2-RT-620 at a scan rate of 0.1 mV s^{-1} and (d) dQ/dV of SnO_2-RT-620 at 0.1C, (e) cycle performance of SnO_2 anodes at 0.1C.

initial capacity of ~1398 mAh g^{-1}, but it rapidly declined within 50 cycles, accompanied by a loss of distinct voltage features, indicating degradation of active material and poor SEI stability. Similarly, the SnO_2-RT sample (black curve) showed a lower initial capacity (~1239 mAh g^{-1}) and even sharper fade, demonstrating that the lack of thermal treatment limits the electrochemical reversibility and structural robustness of the electrode.

The SnO_2-RT-620 sample exhibits markedly lower IR-drop, activation polarization, and overall polarization compared to its non-annealed and 300 °C counterparts, indicating significantly enhanced charge transport and reaction kinetics. In Fig. 2a and b, the blue curves (SnO_2-RT-620) display a noticeably smaller voltage jump at the onset of lithiation, reflecting lower internal resistance likely attributable to improved film conductivity and reduced interface impedance. Concurrently, CV scans in Fig. 2c show sharper, less shifted redox peaks for SnO_2-RT-620, signaling more facile Li^+ insertion/extraction and smaller kinetic barriers. The minimal divergence between its charge and discharge profiles – even after 50 cycles – further confirms its superior overall polarization stability. This contrasts with the larger voltage gaps and broader, shifting peaks seen in SnO_2-RT and SnO_2-300, which suggest higher polarization and SEI instability. Collectively, these results demonstrate that post-deposition air annealing at 620 °C optimizes crystallinity and microstructure, thereby reducing resistance and enabling stable, low-polarization lithiation behavior. From Fig. 4d, a peak splitting and shift reduce over cycles for SnO_2-RT-620 is indicative of low and stable polarization in this sample.

The long-term cycling performance shown in Fig. 2e clearly highlights the superior stability of the SnO_2-RT-620 anode, which retained 710 mAh g^{-1} (46%) after 100 cycles at 0.1C within 0.01–3 V – outperforming all other samples. This result reflects not only high initial capacity but also better structural resilience, stable SEI and minimal side reactions at the electrode–electrolyte interface.[26,27] In contrast, the SnO_2-RT sample showed rapid capacity loss, stabilizing around 20 mAh g^{-1}, likely due to poor film integrity and unstable interfaces. The SnO_2-300 and SnO_2-300-620 samples exhibited intermediate behavior, with the latter showing improved retention owing to post-annealing up to 70 cycles.

3.2. Artificial SEI engineering

Recognizing that SEI behavior is not universal, interface engineering for SnO_2 was pursued. While, for instance, Si-based anodes require flexible, self-healing SEIs, SnO_2 demands a chemically stable interface that resists irreversible lithium loss, particularly from Li_2O formation. To enhance capacity retention and overall electrochemical stability through interface design, the SnO_2 thin film deposited at RT and post-annealed in air – previously referred to as SnO_2-RT-620 – was selected for further study and for convenience renamed SnO_2-bare (Table TS3). Despite its best performance over other investigated anodes, this electrode exhibited gradual fading, likely due to mechanical degradation and/or excessive SEI growth.[21,28]

To suppress parasitic reactions and stabilize the interface, surface modifications were introduced. Specifically, C-coating on SnO_2 films have been applied and tested in 1 M $LiPF_6$ electrolyte (EC : DEC : EMC 1 : 1 : 1) with and without 5 wt% VC.

The SEM images (Fig. 3a and b) clearly show the difference in morphology before and after coating. SnO_2 is characterized by pronounced aggregation and a rough surface. After the deposition of the carbon layer, a denser, fine-grained structure is formed with less visible cracks between clusters. Thus, C-coating reinforced the surface of thin film hidden open SnO_2 sides that is supposed to block extensive reaction of electrolyte with SnO_2. TEM images (Fig. 3c and d) further confirm the presence of an amorphous carbon layer uniformly surrounding the SnO_2 particles. The SnO_2–C sample (Fig. 3d) shows a clear coating of about 20 nm thickness around the periphery of the particles, which serves as direct evidence of shell formation. In contrast, the untreated sample (Fig. 3c) shows an unstructured, less dense surface. Thus, the carbon coating may act as a buffer, reducing side reactions between the electrolyte and the active material.[29] The XRD analysis of SnO_2–C did not reveal characteristic carbon peaks, which is more likely due to its amorphous or nanocrystalline state (refer to Fig. FS2).

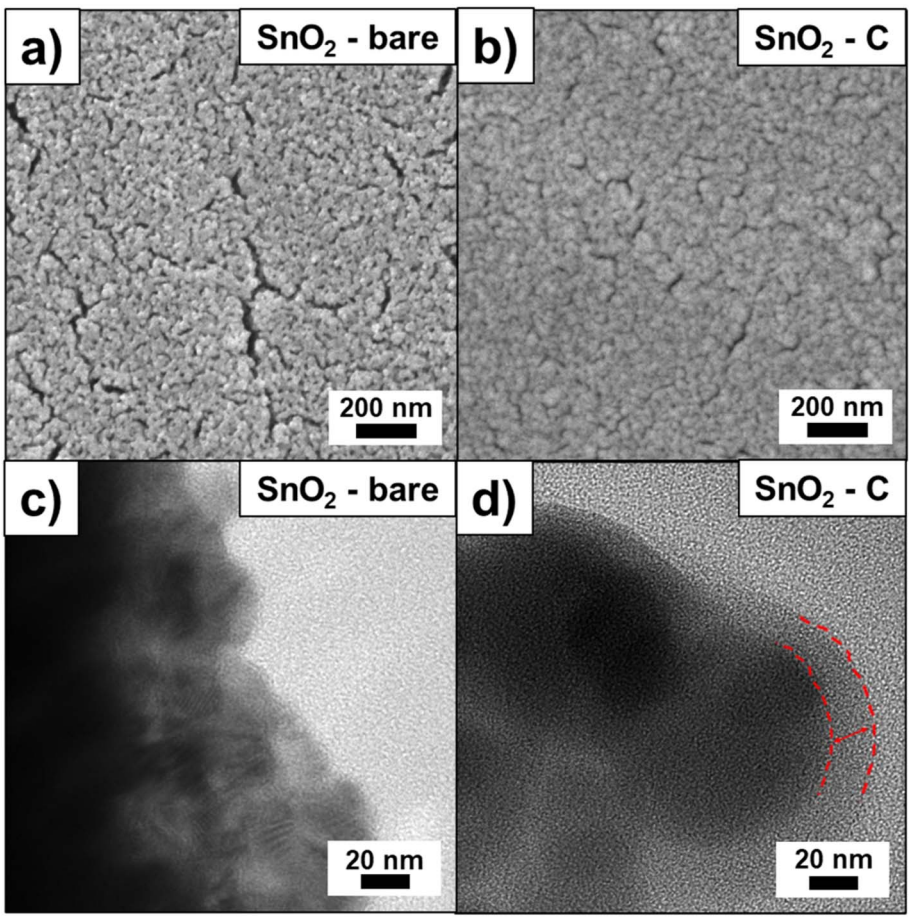

Fig. 3 SEM images of (a) SnO_2-bare, (b) SnO_2–C and TEM image of (c) SnO_2-bare, (d) SnO_2–C thin films.

Fig. 4a–c present the charge–discharge profiles of SnO_2 anodes with different modifications – bare SnO_2 (black), C-coated SnO_2 (red), and C-coated SnO_2 with 5 wt% VC additive (blue) – measured at 0.1C. Already in the initial cycles (Fig. 4a), the advantages of surface engineering become evident: while the bare SnO_2 rapidly develops significant voltage hysteresis, the carbon-coated samples display smoother, more gradual curves. By the 100th cycle (Fig. 4b), the SnO_2–C anode exhibits the most stable and reproducible profile, underscoring the effectiveness of the carbon shell in stabilizing the electrode–electrolyte interface, mitigating SEI growth, and suppressing Sn nanoparticle aggregation.[30] The introduction of VC at this stage brings comparable, though initially less pronounced, benefits.

A striking shift emerges by the 200th cycle (Fig. 4c). While the SnO_2–C electrode begins to lose capacity and shows signs of surface aging – likely due to persistent volumetric changes – the SnO_2–C–VC maintains both its curve shape and capacity retention. This enhancement is attributed to VC's role in forming a stable and elastic SEI during the first cycles, which continues to protect the electrode surface from long-term degradation.[31,32]

This evolution is further clarified in Fig. 4d and FS3, which track the dQ/dV profiles across cycling. All samples exhibit a prominent cathodic peak near 0.8 V in the first cycle, associated with the reduction of SnO_2 to Sn and Li_2O formation, along with lower-potential features for Li_xSn intermetallics. However, only the C-coated samples, particularly with VC, preserve distinct and well-defined dQ/dV peaks throughout 200 cycles – an indicator of robust reaction reversibility and stable structural evolution. In contrast, bare SnO_2 quickly loses these features, reflecting irreversible material degradation and increased impedance.

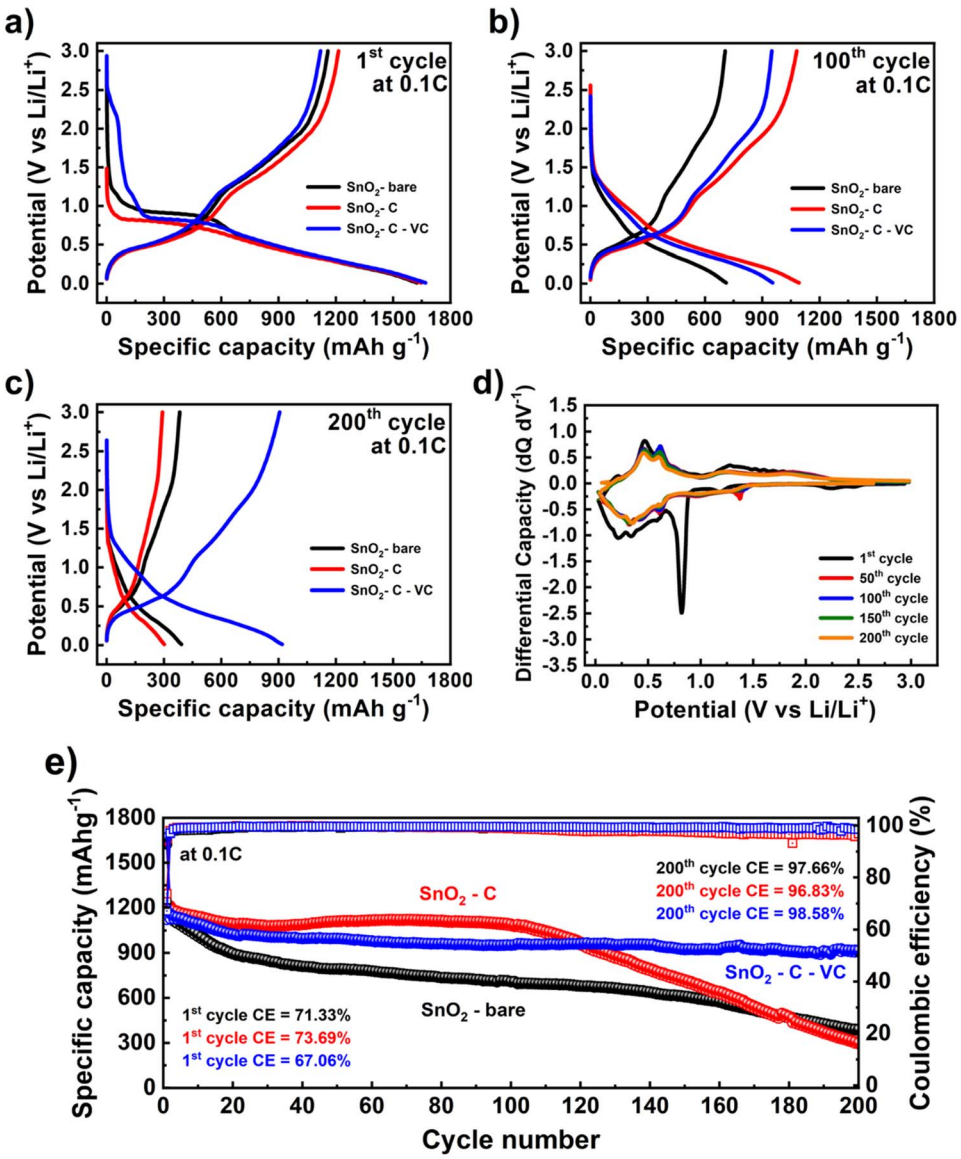

Fig. 4 Potential profiles of SnO_2 anodes at 0.1C at (a) 1st cycle, (b) 100th cycle, (c) 200th cycle and (d) the dQ/dV of anodes and (e) cycle performance of SnO_2 anodes at 0.1C.

Importantly, both C-coated electrodes demonstrate markedly reduced polarization and lower IR drops over time, especially SnO_2–C–VC. Their overlapped potential profiles and minimized voltage offsets (Fig. 4a–c) point to enhanced electronic connectivity, efficient ion transport, and a stable SEI. The dual approach – carbon coating combined with VC – proves synergistic in suppressing both ohmic and activation polarization.

Fig. 4e encapsulates the cumulative impact on long-term cycling. In the first ~20 cycles, all samples generally exhibit a steady decline in capacity. This early capacity decay primarily originates from irreversible processes such as SEI formation, electrolyte decomposition, and partial conversion reactions, which together can be considered an activation process.[14] Following this initial stage, the electrodes generally demonstrate more stable cycling performance. The bare SnO_2 anode suffers a steep capacity decline, dropping from 1623 to just 391 mAh g^{-1}, primarily due to SEI instability and tin aggregation. The SnO_2–C electrode benefits from improved conductivity and surface stabilization, reaching 1091 mAh g^{-1} at 100 cycles, but ultimately declines as by-products accumulate and the carbon shell degrades.[17] In contrast, the SnO_2–C–VC maintains a high and stable capacity of 918 mAh g^{-1} after 200 cycles, with CE consistently above 98% (Fig. FS4). This impressive durability highlights the formation of a robust, elastic SEI mediated by VC, which effectively blocks side reactions and material degradation.

EIS measurements after 200 cycles (Fig. FS5) definitively confirm the beneficial effects of carbon coating and VC additive on interfacial stability and charge transport. The Nyquist plots clearly demonstrate that the bare SnO_2 anode exhibits the largest semicircle and highest total resistance, pointing to substantial interfacial polarization and sluggish ion transfer. In contrast, the SnO_2–C electrode shows a marked reduction in impedance, reflecting improved electronic conductivity and a more stabilized interface due to the protective carbon layer. Most notably, the SnO_2–C–VC sample displays the smallest semicircle and lowest resistance among all samples, indicating the formation of a highly conductive and robust SEI layer enabled by the VC additive. This trend, further emphasized in the low-impedance region (inset), provides compelling evidence that the combined approach of carbon coating and VC incorporation not only mitigates resistive losses at the interface but also ensures efficient ion/electron transport over prolonged cycling.

Thus, the results illustrate that the synergistic combination of carbon coating and VC additive substantially enhances both the structural and electrochemical longevity of SnO_2 anodes, primarily through interfacial stabilization and the suppression of resistive losses.

The post-mortem SEM and XPS analysis were performed to understand the differences in the surface morphology and chemical composition of SEI in the differently modified SnO_2 electrodes after long-term cycling.

SEM images (Fig. 5) reveal that after 200 cycles, the bare SnO_2 anode shows pronounced cracking and surface degradation, consistent with its rapid capacity fade and low efficiency in Fig. 4e. The SnO_2–C electrode retains a more cohesive structure with fewer cracks, while some larger particles observed may arise from the carbon coating, which can encapsulate bigger regions of material but cannot fully accommodate repetitive expansion over cycling—explaining its moderate performance decline. In contrast, SnO_2–C–VC maintains a smooth, intact surface with minimal damage, directly corresponding to its stable capacity and high efficiency. Overall, the enhanced morphology with carbon coating and VC is closely linked to improved cycling stability and durability.

To obtain data on the elemental composition and chemical states of the anodes with SEI, XPS measurements were performed for fresh SnO_2, SnO_2–C (before cycling), and the cycled electrodes after 200 cycles – SnO_2, SnO_2–C, and SnO_2–C–VC (without washing). The obtained spectra are shown in Fig. 6a–f. The Sn 3d spectra after 200 cycles with different coatings (SnO_2–C–VC, SnO_2–C, SnO_2) show two distinct components: Sn $3d_{5/2}$ (~486.5–486.7 eV, red outline) and Sn $3d_{3/2}$ (~494.8–495.0 eV, blue outline) (Fig. 6b), with a characteristic spin–orbit separation of ~8.3 eV, indicating the presence of Sn^{4+} as SnO_2.[33,34] A significant shift of Sn $3d_{5/2}$ to ~485.9 eV was observed, significantly lower than that of oxidized Sn^{4+} (~486.6 eV) and slightly higher than that of metallic Sn^0 (~485.2 eV). This low binding energy may reflect the reduction of Sn^{2+} (SnO) or the formation of a Li–Sn alloy, where the Sn atoms are given excess electron charge from Li.[35] In addition, the spectrum contains a peak at ~487.0 eV with a higher intensity, which most likely corresponds to oxidized forms of Sn, presumably Sn^{4+}, and reflects the incorporation of Sn into SnO_2.[36]

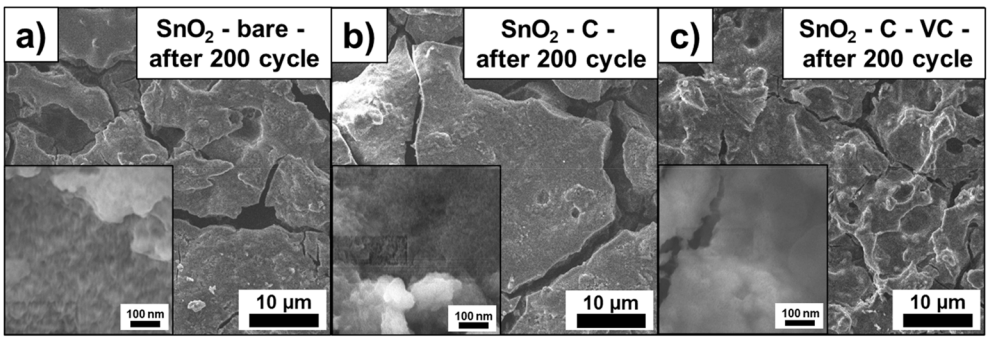

Fig. 5 SEM images of SnO_2 anodes: (a) SnO_2-bare after 200 cycles, (b) SnO_2–C after 200 cycles, and (c) SnO_2–C–VC after 200 cycles.

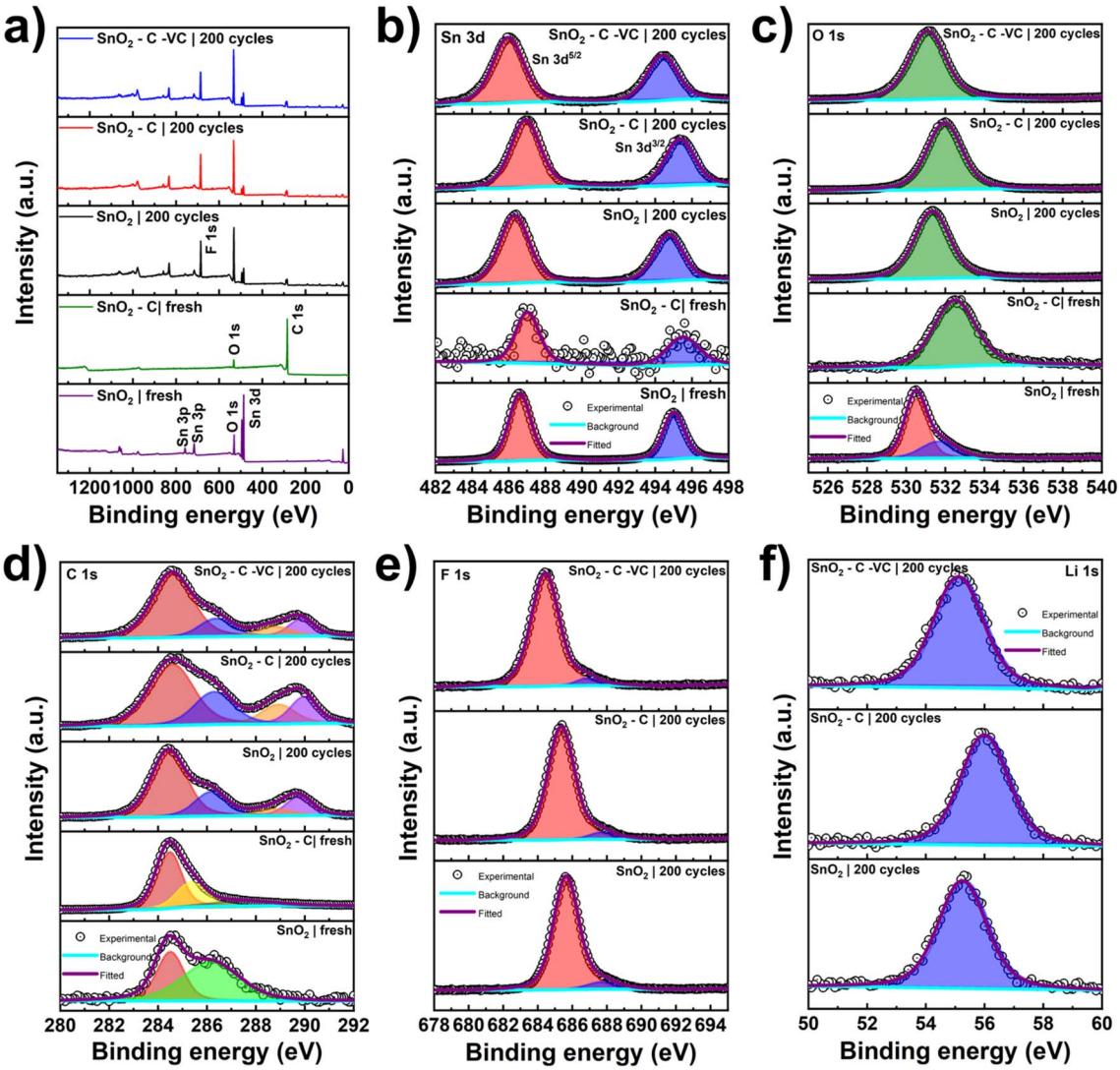

Fig. 6 XPS spectra corresponding to the (a) survey scan, (b) fitted Sn-3d, (c) fitted O 1s spectrum, (d) C 1s, (e) F 1s (f) Li 1s core level regions of SnO_2 anodes before and after cycling.

The main peak of lattice oxygen is at ~530.5 eV, which is typical for heteroatomic oxide thin films SnO_2 with strong Sn–O bonds. After 200 charge–discharge cycles, a peak at ~531.3 eV is observed in the O 1s spectra, which is usually associated with adsorbed surface oxygen (–OH, H_2O) formed on the surface after operation (Fig. 6c).[37,38]

The C 1s spectra show a complex structure (Fig. 6d): the main peak ~284.6–285.0 eV (red) corresponds to C–C/C=C (carbon matrix), the secondary ~286.0 eV (blue) – C–O/C–OH, and ~288.5 eV (violet) – C=O/O–C=O, indicating functional groups/contamination.[39] After cycling, the intensity of the components increases, especially the peak ~286 eV, indicating the accumulation of organic SEI products or carbon decomposition during the process. In the sample with VC, the greatest increase in C–O components occurs, indicating an active interaction with the electrolyte.

The F 1s spectra recorded exclusively for the samples after 200 cycles show three main components at 684.4–685.7 eV (Fig. 6e). These peaks correspond, respectively, to the residual adsorbed fluorophosphate compounds (originating from the electrolyte salt $LiPF_6$ and its decomposition products such as Li_xPF_y, $Li_xPO_yF_z$) and the decomposition product of LiF, which is the key component of the SEI layer. Similarly, Li1s components at 55–56 eV, associated with the deposition of fluorophosphate compounds and LiF, can also be used for this assessment (Fig. 6f). The particularly pronounced Li 1s peak in the SnO_2–C–VC sample confirms the formation of a dense SEI with a high proportion of inorganic lithium fluorides.[40]

The carbon coating significantly enhanced the cycling performance of SnO_2 anodes by protecting surface from excessive electrolyte decomposition, buffering volume changes and improving electrical conductivity. However, SEM analysis (Fig. 5) revealed that over extended cycling, the C-coated SnO_2 develops larger surface particles and shows moderate agglomeration, likely due to the coating's limited ability to accommodate ongoing expansion and contraction. As a result, capacity retention declines after prolonged cycling, indicating partial loss of coating integrity. In contrast, incorporating 5 wt% VC with the

carbon coating yields a much more stable and uniform electrode morphology, with minimal cracking or agglomeration. This improvement, reflected in the sustained high capacity (918 mAh g^{-1}), can be attributed to the formation of a robust, elastic SEI stabilized by VC. Supporting XPS studies confirm that VC increases the fraction of beneficial inorganic LiF in the SEI, reducing side reactions and degradation. Overall, the combined use of carbon coating and VC effectively preserves structural integrity and durability of the SnO_2 anode over long-term cycling.

4 Conclusion

In this study, SnO_2 thin film anodes were fabricated by RF magnetron sputtering, and the effects of deposition conditions and post-annealing on their electrochemical performance were systematically investigated. The SnO_2 film deposited at room temperature and post-annealed in air at 620 °C demonstrated the highest capacity, finer particle size, and superior cycling stability compared to both as-deposited films and those sputtered at higher temperatures.

Engineering an artificial SEI through carbon coating significantly improved cycling performance during the initial 100 cycles by enhancing conductivity and buffering volume changes. However, the durability of this modification was limited upon extended cycling due to gradual loss of coating integrity. Remarkably, the combined strategy of carbon coating with electrolyte modification using 5 wt% VC provided robust long-term protection, leading to outstanding capacity retention. This synergistic approach enabled the formation of a highly conductive and elastic SEI, stabilized by VC, which effectively suppressed side reactions and maintained interface stability.

As a result, the SnO_2–C–VC thin film anodes achieved a stable reversible capacity of approximately 918 mAh g^{-1} with minimal degradation over 200 cycles, while consistently exhibiting coulombic efficiencies around 98%. Post-mortem SEM and XPS analyses confirmed the enhanced structural integrity and favorable SEI chemistry afforded by this dual-modification approach. Overall, these findings underscore the importance of simultaneous morphology and interface engineering for the development of durable, high-performance SnO_2-based anodes for next-generation lithium-ion batteries.

Conflicts of interest

There are no conflicts of interest to declare.

Data availability

All relevant data to support this research is found in the article and the SI. Supplementary information is available. See DOI: https://doi.org/10.1039/d5ra05444c.

Acknowledgements

This research was supported by the project # AP19680567 and the programs # BR21882402, # BR24992766 from the Ministry of Science and Higher Education of the Republic of Kazakhstan.

References

1 A. Manthiram, A reflection on lithium-ion battery cathode chemistry, *Nat. Commun.*, 2020, **11**, 1550, DOI: 10.1038/s41467-020-15355-0.
2 H. Kim, *et al.*, Fast charging of lithium-ion batteries: A review of materials aspects, *Adv. Energy Mater.*, 2021, **11**, 2100150, DOI: 10.1002/aenm.202101126.
3 M. H. Hossain, M. A. Chowdhury, N. Hossain, M. A. Islam and M. H. Mobarak, Advances of lithium-ion batteries anode materials – A review, *Chem. Eng. J. Adv.*, 2023, **16**, 100569, DOI: 10.1016/j.ceja.2023.100569.
4 H. Chang, Y. R. Wu, X. Han and T. F. Yi, Recent developments in advanced anode materials for lithium-ion batteries, *Energy Mater.*, 2021, **1**, 1, DOI: 10.20517/energymater.2021.02.
5 N. Nandihalli, A review of nanocarbon-based anode materials for lithium-ion batteries, *Crystals*, 2024, **14**, 800, DOI: 10.3390/cryst14090800.
6 L. Deng, T. Wei, J. Liu, L. Zhan, W. Chen and J. Cao, Recent developments of carbon-based anode materials for flexible lithium-ion batteries, *Crystals*, 2022, **12**, 1279, DOI: 10.3390/cryst12091279.
7 M. V. Reddy, G. V. Subba Rao and B. V. R. Chowdari, Metal oxides and oxysalts as anode materials for Li ion batteries, *Chem. Rev.*, 2013, **113**, 5364–5457, DOI: 10.1021/cr3001884.
8 S. Schweidler, L. de Biasi, A. Schiele, P. Hartmann, T. Brezesinski and J. Janek, Volume changes of graphite anodes revisited: A combined operando X-ray diffraction and in situ pressure analysis study, *J. Phys. Chem. C*, 2018, **122**, 8829–8835, DOI: 10.1021/acs.jpcc.8b01873.
9 M. Winter, B. Barnett and K. Xu, Before Li ion batteries, *Chem. Rev.*, 2018, **118**, 11433–11456, DOI: 10.1021/acs.chemrev.8b00213.
10 B. Lu, R. Hu, J. Liu, J. Liu, H. Wang and M. Zhu, Improved coulombic efficiency and cycleability of SnO_2–Cu–graphite composite anode with dual scale embedding structure, *RSC Adv.*, 2016, **6**, 13384–13391, DOI: 10.1039/C5RA23988E.
11 J. Guo, P. Li, L. Chai, Y. Su, J. Diao and X. Guo, Silica template-assisted synthesis of SnO_2@porous carbon composites as anode materials with excellent rate capability and cycling stability for lithium-ion batteries, *RSC Adv.*, 2017, **7**, 30070–30079, DOI: 10.1039/C7RA03594B.
12 A. Serikkazyyeva, A. Mashekova, B. Uzakbaiuly, Z. Bakenov and A. Mukanova, Novel Li/Li_xSn_y thin film designed as an anode for lithium-ion microbatteries, *J. Alloys Compd.*, 2023, **965**, 171381, DOI: 10.1016/j.jallcom.2023.171381.
13 X. Liu, M. Li, C. Shi, S. An, J. Wang and S. Yao, Sn/SnO_2/C prepared by carbothermal reduction method as the anode material for sodium-ion batteries, *J. Electron. Mater.*, 2025, **54**, 2735–2746, DOI: 10.1007/s11664-025-11765-2.
14 S. J. An, J. Li, C. Daniel, D. Mohanty, S. Nagpure and D. L. Wood III, The state of understanding of the lithium-ion-battery graphite solid electrolyte interphase (SEI) and its relationship to formation cycling, *Carbon*, 2016, **105**, 52–76, DOI: 10.1016/j.carbon.2016.04.008.

15 T. Yang and B. Lu, Highly porous structure strategy to improve the SnO_2 electrode performance for lithium-ion batteries, *Phys. Chem. Chem. Phys.*, 2014, **16**, 4115–4121, DOI: 10.1039/C3CP54144D.

16 K. Y. Chan and B. S. Teo, Sputtering power and deposition pressure effects on the electrical and structural properties of copper thin films, *J. Mater. Sci.*, 2005, **40**, 5971–5981, DOI: 10.1007/s10853-005-1362-8.

17 Y. Zhang, H. Zhang, J. Zhang, J. Wang and Z. Li, Carbon-coated SnO_2 thin films developed by magnetron sputtering as anode material for lithium-ion batteries, *RSC Adv.*, 2015, **5**, 106258–106264, DOI: 10.1039/C5RA21457B.

18 A. Mukanova, A. Serikkazyyeva, A. Nurpeissova, S. S. Kim, M. Myronov and Z. Bakenov, Understanding the effect of p-, n-type dopants and vinyl carbonate electrolyte additive on electrochemical performance of Si thin film anodes for lithium-ion battery, *Electrochim. Acta*, 2020, **330**, 135179, DOI: 10.1016/j.electacta.2019.135179.

19 J. Lu, M. Sundqvist, A. Ottosson, A. Tarre, A. Rosental, J. Aarik and A. Hårsta, Microstructure characterisation of ALD-grown epitaxial SnO_2 thin films, *J. Cryst. Growth*, 2004, **260**, 191–200, DOI: 10.1016/j.jcrysgro.2003.08.042.

20 Y. Kong, Z. Ma, Y. Ye, G. He, Y. Sun, X. Zuo and J. Nan, Nanosized amorphous SnO_2 particles anchored in the wheat straw carbon substrate as the stabilized anode material of lithium-ion batteries, *ACS Appl. Energy Mater.*, 2018, **1**, 7065–7075, DOI: 10.1021/acsaem.8b01408.

21 R. Kajal, B. R. Kataria, K. Asokan and D. Mohan, Effects of gamma radiation on structural, optical, and electrical properties of SnO_2 thin films, *Appl. Surf. Sci. Adv.*, 2023, **15**, 100406, DOI: 10.1016/j.apsadv.2023.100406.

22 T. Kobayashi, *et al.*, Process of crystallization in thin amorphous tin oxide film, *J. Cryst. Growth*, 2002, **243**, 143–150, DOI: 10.1016/S0022-0248(02)01445-8.

23 S. B. Ghantasala and S. Sharma, Magnetron sputtered thin films based on transition metal nitride: structure and properties, *Phys. Status Solidi A*, 2023, **220**, 2200229, DOI: 10.1002/pssa.202200229.

24 S. Kim, D. H. Kim and S. H. Hong, Epitaxial growth of orthorhombic SnO_2 films on various YSZ substrates by plasma enhanced atomic layer deposition, *J. Cryst. Growth*, 2012, **348**, 15–19, DOI: 10.1016/j.jcrysgro.2012.03.047.

25 Y. Idota, T. Kubota, A. Matsufuji, Y. Maekawa and T. Miyasaka, Tin-based amorphous oxide: a high-capacity lithium-ion-storage material, *Science*, 1997, **276**, 1395, DOI: 10.1126/science.276.5317.1395.

26 L. Ding, S. He, S. Miao, M. R. Jorgensen, S. Leubner, C. Yan, *et al.*, Ultrasmall SnO_2 nanocrystals: hot-bubbling synthesis, encapsulation in carbon layers and applications in high capacity Li-ion storage, *Sci. Rep.*, 2014, **4**, 4647, DOI: 10.1038/srep04647.

27 X. Zhu, Y. Zhu, S. Murali, M. D. Stoller and R. S. Ruoff, Reduced graphene oxide/tin oxide composite as an enhanced anode material for lithium-ion batteries prepared by homogenous coprecipitation, *J. Power Sources*, 2011, **196**, 6473–6477, DOI: 10.1016/j.jpowsour.2011.04.015.

28 Y. Ma, X. Zhang, W. Liu, Y. Wei, Z. Fu, J. Li and Y. Yan, Stoichiometry dependence of physical and electrochemical properties of the SnO_x film anodes deposited by pulse DC magnetron sputtering, *Materials*, 2021, **14**, 1803, DOI: 10.3390/ma14071803.

29 S. Maharajan, N. H. Kwon, P. Brodard and K. M. Fromm, A nano-rattle SnO_2@carbon composite anode material for high-energy Li-ion batteries by melt diffusion impregnation, *Nanomaterials*, 2020, **10**, 804, DOI: 10.3390/nano10040804.

30 A. Gupta, *et al.*, High rate capability and cyclic stability of hierarchically porous tin oxide (IV)-carbon nanofibers as anode in lithium-ion batteries, *Appl. Nanosci.*, 2017, **7**, 449–462, DOI: 10.1007/s13204-017-0577-8.

31 Y. Li, *et al.*, A nanoscale interlayer void design enabling high-performance SnO_2-carbon anodes, *Carbon*, 2021, **183**, 486–494, DOI: 10.1016/j.carbon.2021.06.089.

32 X. Lan, *et al.*, Insight into reversible conversion reactions in SnO_2-based anodes for lithium storage: A review, *Small*, 2022, **18**, 2201110, DOI: 10.1002/smll.202201110.

33 J. Saddique, *et al.*, Synthesis and characterization of Sn/SnO_2/C nano-composite structure: high-performance negative electrode for lithium-ion batteries, *Materials*, 2022, **15**, 2475, DOI: 10.3390/ma15072475.

34 E. Jiang, Y. Ai, J. Yan, N. Li, L. Lin, Z. Wang and J. Ye, Phosphate-passivated SnO2 electron transport layer for high-performance perovskite solar cells, *ACS Appl. Mater. Interfaces*, 2019, **11**, 36727–36734, DOI: 10.1021/acsami.9b11817.

35 J. T. Li, J. Swiatowska, A. Seyeux, L. Huang, V. Maurice, S. G. Sun and P. Marcus, XPS and ToF-SIMS study of Sn-Co alloy thin films as anode for lithium ion battery, *J. Power Sources*, 2010, **195**, 8251–8257, DOI: 10.1016/j.jpowsour.2010.07.043.

36 A. Birrozzi, A. Mullaliu, T. Eisenmann, J. Asenbauer, T. Diemant, D. Geiger and D. Bresser, Synergistic effect of Co and Mn co-doping on SnO_2 lithium-ion anodes, *Inorganics*, 2022, **10**, 46, DOI: 10.3390/inorganics10040046.

37 Y. Yu, L. Gu, A. Dhanabalan, C. H. Chen and C. Wang, Three-dimensional porous amorphous SnO_2 thin films as anodes for Li-ion batteries, *Electrochim. Acta*, 2009, **54**, 7227–7230, DOI: 10.1016/j.electacta.2009.07.028.

38 G. Kiruthiga, K. S. Rajni, N. Geethanjali, T. Raguram, E. Nandhakumar and N. Senthilkumar, SnO_2: Investigation of optical, structural, and electrical properties of transparent conductive oxide thin films prepared by nebulized spray pyrolysis for photovoltaic applications, *Inorg. Chem. Commun.*, 2022, **145**, 109968, DOI: 10.1016/j.inoche.2022.109968.

39 Y. Bourlier, M. Bouttemy, O. Patard, P. Gamarra, S. Piotrowicz, J. Vigneron and A. Etcheberry, Investigation of InAlN layers surface reactivity after thermal annealings: a complete XPS study for HEMT, *ECS J. Solid State Sci. Technol.*, 2018, **7**, P329, DOI: 10.1149/2.0181806jss.

40 S. Ivanov, S. Mai, M. Himmerlich, A. Dimitrova, S. Krischok and A. Bund, Microgravimetric and spectroscopic analysis of solid–electrolyte interphase formation in presence of additives, *ChemPhysChem*, 2019, **20**, 655–664, DOI: 10.1002/cphc.201801001.